Journal of Sound and Vibration 382 (2016) 1–12

Contents lists available at ScienceDirect

Journal of Sound and Vibration

journal homepage: www.elsevier.com/locate/jsvi

Estimation of the transient response of a tuned, fractionally damped elastomeric isolator

Luke Fredette, Rajendra Singh *

Acoustics and Dynamics Laboratory, Smart Vehicle Concepts Center, Department of Mechanical and Aerospace Engineering, The Ohio State University, Columbus, OH 43210, USA

ARTICLE INFO

Article history:
Received 9 March 2016
Received in revised form
6 June 2016
Accepted 6 July 2016
Handling Editor: H. Ouyang
Available online 22 July 2016

Keywords:
Fractional Calculus
Viscoelastic Isolator
Transient Response
Analytical Methods
Passive Vibration Control

ABSTRACT

This article addresses the frequency dependent properties of elastomeric vibration isolators in the context of lumped parameter models with fractional damping elements. A mass is placed between two fractional calculus Kelvin-Voigt elements to develop a minimal order system for the example case of a conventional elastomeric bushing typical of automotive suspension systems. Model parameters are acquired from measured dynamic stiffness spectra and a finite element model. The minimal order system model accurately predicts dynamic stiffness in both broadband resonant behavior as well as the lower-frequency regime that is controlled by damping. For transient response analysis, an inverse Laplace transform of the dynamic stiffness spectrum is taken via the Residue Theorem. Since the fractional calculus based solution is given in terms of problematic integrals, a new time-frequency domain estimation technique is proposed which approximates time-domain responses for a class of transient excitation functions. The approximation error is quantified and found to be reasonably small, and tractable closed-form transient response functions are provided along with a discussion of numerical issues.

1. Introduction

Elastomeric isolators, mounts, and bushings are widely used in machines, vehicles, and buildings. In automotive suspension, for instance, bushings are used extensively to ensure vibration isolation and impedance mismatch between critical subsystems. Such isolators have been analytically studied with continuous system theory [1–3] as well as lumped parameter models on both the component [4–6] and system [7] level, often with many simplifications. In many cases, isolators exhibit nonlinear behavior [3–5,8] which may be more readily apparent from transient responses [4,5]. In recent decades, increased attention has been given to the use of fractional order derivatives to describe the viscoelastic behavior of elastomeric materials [9–14]. Fractional calculus theory has many physical applications [9,10] and has been applied to viscoelasticity in the context of pure constitutive relations [10–13], material models suitable for finite element analysis [12], and lumped system modeling [14,15]. Despite the many approaches to using fractional calculus for viscoelasticity [10], it is still not widely used in practice, presumably due to the difficulty of the mathematical sophistication which is often required to produce useful results. Prior approaches to employ fractional calculus can be divided into two categories: analytical

* Corresponding author.
E-mail address: singh.3@osu.edu (R. Singh).

http://dx.doi.org/10.1016/j.jsv.2016.07.009
0022-460X/

transformations of fractional calculus formulations based on Cauchy integrals [9–11,13,14] and those numerical estimation of fractional derivatives based on the variations of the Grünwald definition [9,10,12,15]. Each methodology presents unique strengths and weaknesses, but this article aims to adopt and build on the analytical approach by introducing an estimation procedure which may simplify the difficult time-domain transformation calculations [13,14], extending the method to a new class of system. The chief goal is to develop semi-analytical, time-domain response estimates to a class of transient excitation signals when applied to a tuned elastomeric isolator (with inertial effects) in the context of a minimal order model.

2. Problem formulation

Elastomeric isolation components used in automotive suspension exhibit significant frequency-dependent stiffness behavior over a wide range of frequencies. Such "tuned" properties result from inertial and damping effects in the material, each being dominant in a different frequency regime. Capturing the relevant physics in a reduced-order, lumped-parameter model which is effective over a broad frequency range is challenging. Recently, Noll, et al. developed a lumped parameter model for an elastomeric joint which clarified the frequency-dependent stiffness by capturing internal mass effects [6]. Their model offers good broadband dynamic stiffness predictions, but significant error is found in the lower-frequency regime (say, up to 100 Hz). This error is linked to the damping mechanism assumed in the model [6]. Neither structural nor viscous damping is able to produce the low-frequency behavior with a minimal-order model [15], although large, empirical viscoelastic networks may reproduce the effect on an *ad hoc* basis. A damping mechanism based on fractional calculus is expected to yield superior predictions as assumed in this article.

The objectives of this article are as follows: 1. Develop a uniaxial minimal order model which can effectively simulate the dynamic stiffness of a production bushing, capturing both low-frequency and broadband behavior covering the first resonance (0–1 kHz), and 2. Propose a new estimation technique to yield time-domain solution approximations for transient excitation using fractional calculus. Spectral characterization of such viscoelastic isolators is useful but insufficient, as the assumption of purely harmonic excitation is unrealistic and may mask properties of the elastomeric system that are relevant under aperiodic or transient excitation. Studying transient responses requires a time-domain representation of the system, such as an impulse response function. Fractional dampers preclude conventional inverse Laplace transform calculations to obtain the impulse response; however, the transform may be obtained using the Residue Theorem and multi-domain estimation techniques. The step response is useful in the analysis of elastomeric isolators since it includes an abrupt shift in the operating loads which may excite interesting behavior from any amplitude-dependent nonlinearities in the system [3,5,10,12,15]. Determination of such amplitude-dependent behavior is beyond the scope of this work; nevertheless, a "step-like" input will be used as an example for a realistic transient excitation. Additional complexities may be observed in elastomeric materials such as temperature dependence, aging effects, and anisotropy [16]. Since dynamic behavior of viscoelastic materials often exhibit limited sensitivity to these effects for small perturbations about an operating point, these are beyond the scope of this work.

3. Spectral characterization and minimal order model

Elastomeric isolators are typically characterized in terms of dynamic stiffness spectra [1–3,6,7]. A comparison between the measured cross-point stiffness magnitude spectrum and finite element predictions of a laboratory bushing (very similar to production devices [6]) is given in Fig. 1. Details and parameters of the finite element model are already reported in [6]. Good broadband accuracy is achieved by the finite element model; however, at low frequencies (below 100 Hz), the measurement reveals a damping mechanism which is not incorporated in the model. Conversely, the measured dynamic stiffness spectrum only goes up to 600 Hz (due to the limitations of the dynamic elastomer test machine), whereas finite element models can extend to larger bandwidths to capture stiffness peaks due to the internal mass. Fig. 2 depicts the simulated dynamic stiffness spectra for a production bushing [6], including both driving-point and cross-point stiffness

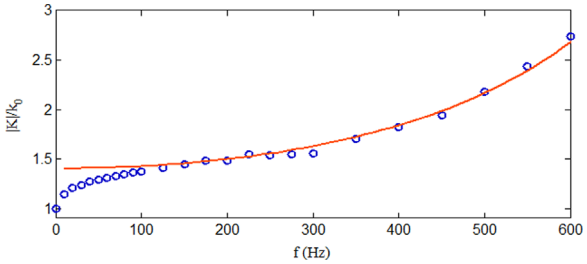

Fig. 1. Dynamic stiffness predictions of an elastomeric isolator showing insufficiency of structural damping mechanism available in finite element model [6]. Key: ○ - Measurement; ▬ - Finite element model with structural damping.

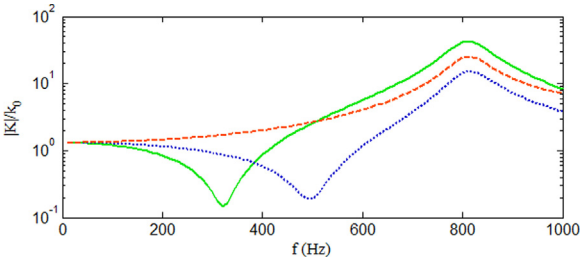

Fig. 2. Dynamic stiffness terms of Eq. (2) using a finite element model [6] of a production bushing with structural damping. Key: ••••• - K_{11}; ▬ ▬ ▬ - K_{12}; ▬▬ - K_{22}.

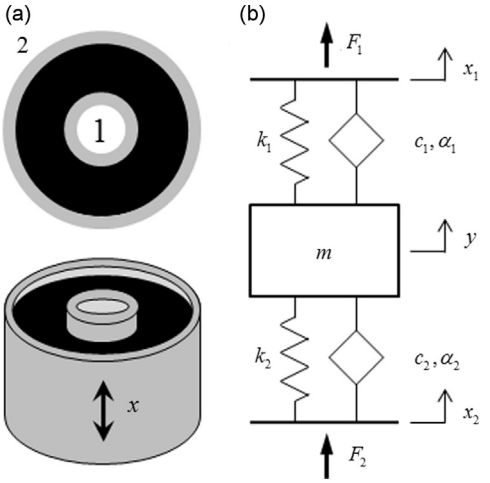

Fig. 3. Example case for the isolator study: (a) schematic of the elastomeric bushing with inner (1) and outer (2) sleeves and viscoelastic material shown in dark color. Only the axial direction is considered. (b) The proposed minimal order model. Here, x_1, x_2, and F_1, F_2 are the displacements and forces of the inner and outer metallic sleeves, respectively. The effective internal mass of the elastomeric material is m, and y is its displacement. The spring constants k_1 and k_2 denote the stiffness of the elastic elements whilec_1,c_2 and α_1,α_2 denote the fractional damper coefficients and order parameters, respectively.

curves. A model framework which can predict the broadband dynamics while capturing the measured low-frequency behavior observed in Fig. 1 would be quite useful.

A minimal order model of a rubber bushing, as shown schematically in Fig. 3(a), is proposed to capture the stiffness, mass, and damping properties. Here, the 1 and 2 coordinates represent the inner and outer metal sleeves the bushing, assumed to be rigid compared to the elastomeric material. Fig. 3(b) shows the minimal order model using the four-pole type representation with arbitrary boundaries [17]. The governing equations (with fractional damping elements) are given by,

$$m\ddot{y}+(k_1+c_1D_t^{\alpha_1})y(t)+(k_2+c_2D_t^{\alpha_2})y(t)=(k_1+c_1D_t^{\alpha_1})x_1(t)+(k_2+c_2D_t^{\alpha_2})x_2(t), \tag{1-a}$$

$$F_1(t)=(k_1+c_1D_t^{\alpha_1})(y(t)-x_1(t)), \tag{1-b}$$

$$F_2(t)=(k_2+c_2D_t^{\alpha_2})(y(t)-x_2(t)), \tag{1-c}$$

where x_1, x_2, F_1, and F_2 are the displacements and forces of the inner and outer sleeves, respectively. (Also see Appendix A for the identification of symbols.) The m parameter is the effective internal mass of the elastomeric material, representing the effective inertia that participates in the first vibration mode (analogous to a modal mass). The corresponding displacement coordinate is given as y. Fractional Kelvin-Voigt elements characterize the viscoelastic behavior. The spring constants k_1 and k_2 denote the stiffness of the elastic elements connecting the internal mass to each boundary. The constitutive equations for the two fractional dampers relate dissipative path force to a fractional derivative of displacement, $F=cD_t^{\alpha}x$, where D_t^{α} is a derivative operator of order α with respect to t. Therefore, the fractional dampers have four parameters in all: coefficients (c_1,c_2) and order parameters (α_1,α_2).

Assuming harmonic excitation, driving point (K_{11},K_{22}) and cross-point (K_{12},K_{21}) dynamic stiffness terms for the system of Fig. 3(b) are defined in the Laplace domain as,

$$K_{11}(s)=\frac{F_1}{x_1}\bigg|_{x_2=0}=\frac{(k_1+c_1s^{\alpha_1})^2}{ms^2+c_1s^{\alpha_1}+c_2s^{\alpha_2}+k_1+k_2}-1, \tag{2-a}$$

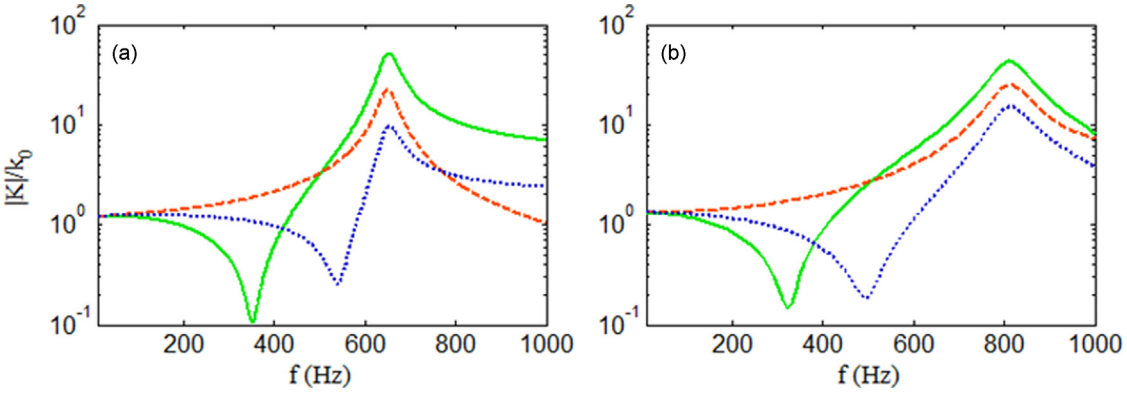

Fig. 4. Dynamic stiffness spectra predicted from the (a) minimal order model and (b) finite element model [6]. Two frequency regimes emerge below and above 100 Hz. The two models agree qualitatively in terms of broadband behavior. Key: ••••• - K_{11}; - K_{12}; - K_{22}.

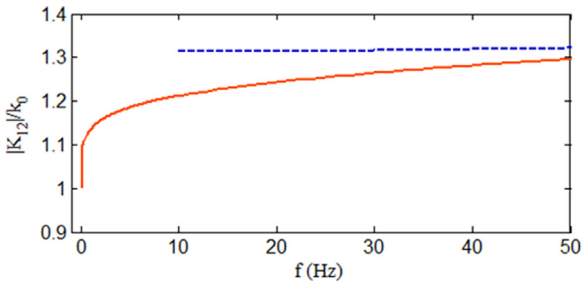

Fig. 5. Low-frequency behavior of the minimal order model, capturing the damping-controlled convergence to static stiffness while the finite element predictions fail to capture the behavior. Key: - Minimal order model; - Finite element model [6].

$$K_{22}(s)=\left.\frac{F_2}{x_2}\right|_{x_1=0}=\frac{(k_2+c_2s^{\alpha_2})^2}{ms^2+c_1s^{\alpha_1}+c_2s^{\alpha_2}+k_1+k_2}-1, \tag{2-b}$$

$$K_{12}(s)=K_{21}(s)=\left.\frac{F_2}{x_1}\right|_{x_2=0}=\frac{(k_1+c_1s^{\alpha_1})(k_2+c_2s^{\alpha_2})}{ms^2+c_1s^{\alpha_1}+c_2s^{\alpha_2}+k_1+k_2}. \tag{2-c}$$

Fig. 4 shows plots of the dynamic stiffness terms using assumed, yet realistic model parameters derived from curve-fitting typical measured stiffness spectra with Eqs. (2-a,b,c), where the dynamic magnitude is normalized by the corresponding static stiffness, $k_0=k_1k_2/(k_1+k_2)$. The minimal order model predictions qualitatively agree with finite element predictions (of [6], in Fig. 4) in terms of resonance behavior; however, whereas finite element predictions fail to capture the low-frequency trend, the proposed model produces low-frequency behavior that is similar to the measurements (as shown in Fig. 5) by using fractional dampers instead of structural damping (in the form of a loss factor).

4. Time domain characterization

An impulse response function can be calculated from any of the dynamic stiffness expressions,

$$h(t)=\mathcal{L}^{-1}\{K(s)\}, \tag{3}$$

using the inverse Laplace transform,

$$\mathcal{L}^{-1}\{K(s)\}=\frac{1}{2\pi i}\lim_{R\to\infty}\int_{\xi-iR}^{\xi+iR}K(s)e^{st}ds, \tag{4}$$

which is a contour integral in the complex plane, and ξ is a positive, real offset. The Residue Theorem relates a contour integral along a closed loop C to the residues of all singular points λ_j of the function enclosed by the loop,

$$\int_C K(s)e^{st}ds=2\pi i\sum_j \mathrm{Res}\left[K(s)e^{st},\lambda_j\right], \tag{5-a}$$

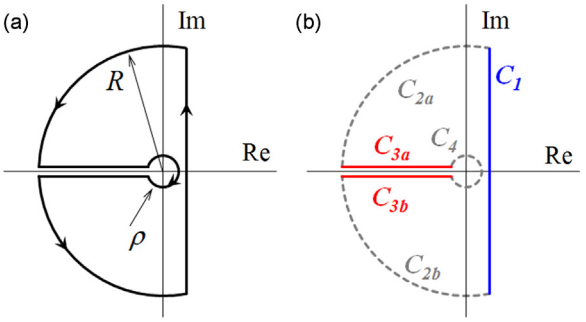

Fig. 6. Application of the Residue Theorem showing (a) the Bromwich contour used to evaluate the inverse Laplace transform and (b) division of the contour into zero and nonzero segments. Key: ▬ - Bromwich contour; ▬ ▬ ▬ - Integrals sum to zero; ▬ - Inverse Laplace transform segment; ▬ - Remaining segments.

$$\mathrm{Res}\left[K(s)\mathrm{e}^{st},\lambda_j\right]=\lim_{s\to\lambda_j}(s-\lambda_j)K(s)\mathrm{e}^{st}. \tag{5-b}$$

If C encloses any branch points of $K(s)$, then the integrand's discontinuity will violate the conditions of the theorem. Fractional damping elements generate a branch point at the origin, so the contour is judiciously chosen to avoid it as seen in Fig. 6(a). Jordan's lemma demonstrates that as $R\to\infty$ and $\rho\to 0$, the integrals along the contours C_{2a}, C_{2b}, and C_4 vanish, leaving three remaining terms as shown in Fig. 6(b),

$$\int_C \mathrm{K(s)e^{st}ds}=\int_{C_1}K(s)\mathrm{e}^{st}\mathrm{d}s+\int_{C_{3a}}K(s)\mathrm{e}^{st}\mathrm{d}s+\int_{C_{3b}}K(s)\mathrm{e}^{st}\mathrm{d}s. \tag{6}$$

Since the contour C_1 is equivalent to the transform integral from Eq. (4), it follows from (4), (5-a), and (6) that

$$h(t)=\sum_j \mathrm{Res}\left[K(s)\mathrm{e}^{st},\lambda_j\right]-\frac{1}{2\pi\mathrm{i}}\left(\int_{C_{3a}}K(s)\mathrm{e}^{st}\mathrm{d}s+\int_{C_{3b}}K(s)\mathrm{e}^{st}\mathrm{d}s\right). \tag{7}$$

Observe that the two terms of $h(t)$ are quite different, and thus they are defined individually as,

$$h(t)=h_v(t)+h_r(t), \tag{8}$$

where h_v is the sum of the residues and h_r is the remaining integral term. Although it is not obvious from Eq. (7), the two terms are named in this manner because the residues yield a vibratory response while the integrals produce a relaxation effect as illustrated in the next two sections.

5. Vibratory response

The vibratory response is given as the sum of the residues of $K(s)\mathrm{e}^{st}$ in (7) which requires that any singular points contained in the region bounded by C are located. Singular points occur at the zeros of the $K(s)$ denominator $Z(s)=ms^2+c_1s^{\alpha_1}+c_2s^{\alpha_2}+k_1+k_2$, which (unlike the simple harmonic oscillator systems with viscous damping) is a fractional polynomial. Given complications in root-finding calculations, several approaches may be used to locate these roots. First, assume that both fractional order parameters are rational ($\alpha_1=q_1/n$, $\alpha_2=q_2/n$, where q_1, q_2, and n are integers) and defining a second Laplace variable, $p=s^{1/n}$. Z is now converted to a more conventional polynomial,

$$Z=ms^2+c_1s^{\alpha_1}+c_2s^{\alpha_2}+k_1+k_2=mp^{2n}+c_1p^{q_1}+c_2p^{q_2}+k_1+k_2. \tag{9}$$

The roots may be calculated by generating a Frobenius companion matrix [18] and calculating its eigenvalues. This yields the $2n$ roots of the right hand side of Eq. (9), which should collapse to the two roots of the left hand side, $\lambda_s=\lambda_p^n$. However, an unacceptable degree of error may creep into the calculation of companion matrix eigenvlaues for a large n (which may become quite large for arbitrary fractional order parameters), and thus the roots λ_p may fail to collapse to just two roots λ_s. Due to the inherent extreme behavior of $K(s)$ near these roots, the residues may be sensitive to the error in singular point values, and therefore an alternate technique is proposed below.

The Newton–Raphson Method is a classical approach for both root-finding and minimization problems. Although it is an iterative approach, this method can locate a function's roots in the complex plane with high precision after only a few steps given a well-behaved function and a good initial guess. As it happens, the example case in this article offers both. For $0<\alpha_1,\alpha_2<1$, there are always two complex-conjugate roots in the left half-plane. Selection of an initial guess in quadrant II (e.g. $s_0=-1+\mathrm{i}$) leads to a quick convergence to the singular point in that quadrant with a very high degree of precision, as shown in Fig. 7.

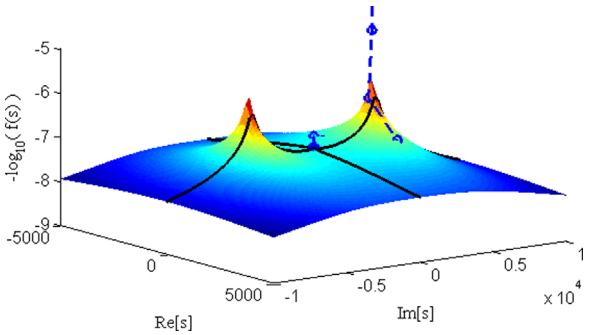

Fig. 7. Minimization procedure using the Newton–Raphson Method to locate singular points in the transfer function. Key: ○ - Approximate singular point location; ▬ ▬ ▬ - Path of Newton–Raphson Method.

Once the singular points λ_s, λ_s^* are calculated, the residues may be evaluated. For the cross-point dynamic stiffness, the residue from Eq. (2-c) is,

$$\mathrm{Res}\left[K(s)\mathrm{e}^{st}, \lambda_s\right] = \lim_{s\to\lambda_s} \frac{(s-\lambda_s)(k_1+c_1 s^{\alpha_1})(k_2+c_2 s^{\alpha_2})}{ms^2+c_1 s^{\alpha_1}+c_2 s^{\alpha_2}+k_1+k_2}\mathrm{e}^{st}, \tag{10}$$

which yields an indeterminate form. Application of L'Hopital's rule leads to a simplified solution as,

$$\mathrm{Res}\left[K(s)\mathrm{e}^{st}, \lambda_s\right] = \frac{\left(k_1+c_1\lambda_s^{\alpha_1}\right)\left(k_2+c_2\lambda_s^{\alpha_2}\right)}{2ms+\alpha_1 c_1\lambda_s^{\alpha_1-1}+\alpha_1 c_2\lambda_s^{\alpha_2-1}}\mathrm{e}^{\lambda_s t} = (A+iB)e^{(a+\mathrm{i}b)t}, \tag{11-a}$$

$$\mathrm{Res}\left[K(s)\mathrm{e}^{st}, \lambda_s^*\right] = (A-\mathrm{i}B)\mathrm{e}^{(a-\mathrm{i}b)t}, \tag{11-b}$$

where a, b are the real and imaginary parts of the quadrant III singular point and A, B are the real and imaginary parts of its residue, respectively. The vibratory impulse response $h_v(t)$ is now calculated,

$$h_v(t) = (A+\mathrm{i}B)\mathrm{e}^{(a+\mathrm{i}b)t} + (A-\mathrm{i}B)\mathrm{e}^{(a-\mathrm{i}b)t}, \tag{12}$$

and rewritten as,

$$h_v(t) = 2\sqrt{A^2+B^2}\mathrm{e}^{at}\ \sin(bt+\theta), \tag{13-a}$$

$$\theta = \tan^{-1}\left(\frac{A}{-B}\right). \tag{13-b}$$

6. Relaxation response

The second term of the impulse response function in Eq. (7) is somewhat more difficult to calculate. The integrals can be simplified by letting $s = \ell e^{\mathrm{i}\pi}$ on C_{3a} and $s = \ell e^{-\mathrm{i}\pi}$ on C_{3b},

$$h_r(t) = -\frac{1}{2\pi\mathrm{i}}\lim_{\rho\to 0}\lim_{R\to\infty}\int_\rho^R \left(K\left(\ell\mathrm{e}^{\mathrm{i}\pi}\right) - K\left(\ell\mathrm{e}^{-\mathrm{i}\pi}\right)\right)\mathrm{e}^{-\ell t}\mathrm{d}\ell. \tag{14}$$

Using (2-c) in (14) yields,

$$h_r(t) = -\frac{1}{\pi\mathrm{i}}\int_0^\infty \mathrm{Im}\left[K\left(\ell\mathrm{e}^{\mathrm{i}\pi}\right)\right]\mathrm{e}^{-\ell t}\mathrm{d}\ell, \tag{15}$$

which cannot be evaluated by conventional integration techniques. While it is always possible that a solution to this integral exists, any significant modifications to $K(s)$ would likely require new analytical solutions, so an alternate approach is suggested. Decompose $K(s)$ into vibratory and relaxation terms by taking the Laplace transform of Eq. (8) as shown in Fig. 8,

$$K_r(s) = K(s) - \mathcal{L}\{h_v(t)\}. \tag{16}$$

The plot of Fig. 8 illustrates that $K_v(s)$ is itself a relatively crude approximation of $K(s)$, while the effects of $K_r(s)$ are an order of magnitude smaller except at the very low frequency end. Nevertheless, capturing such low-frequency behavior is among the benefits of using fractional damping in a reduced order model. The algebraic expression for $K_r(s)$ is quite complicated and would not always have a convenient inverse Laplace transform. As such, the following two-parameter

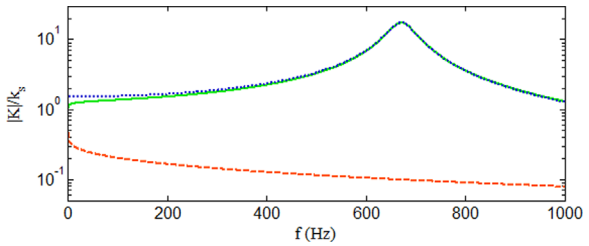

Fig. 8. Spectral components of the dynamic stiffness where the vibratory stiffness term may serve as a rough estimate of the total dynamic stiffness. Key: ——— - Total dynamic stiffness, K; • • • • • - Vibratory dynamic stiffness, K_v; — — — - Relaxation dynamic stiffness, K_r.

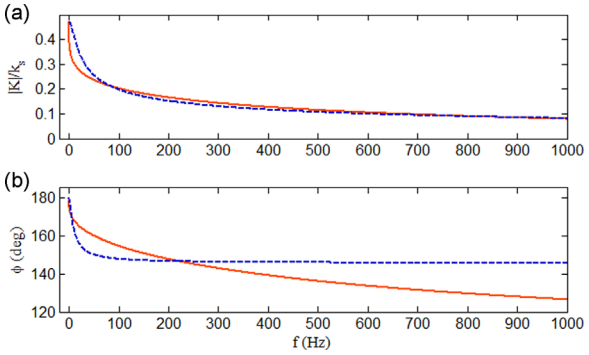

Fig. 9. Estimation of the relaxation stiffness component in terms of (a) magnitude and (b) phase. Key: ——— - $K - K_v$; — — — - $\hat{K}_r$.

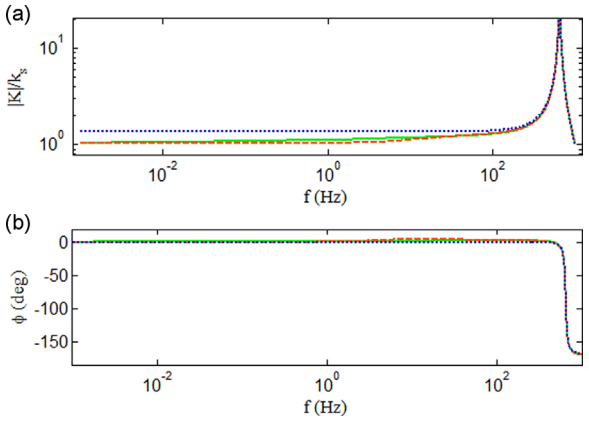

Fig. 10. Dynamic stiffness estimation in terms of (a) magnitude and (b) phase. Key: • • • • • - Vibratory dynamic stiffness, K_1; — — — - Total dynamic stiffness estimate, $\hat{K}_r$; ——— - True dynamic stiffness, K_r.

functional approximation is proposed to yield similar behavior with greatly simplified calculations,

$$\hat{K}_r(s) = \frac{h_{20}}{(s-\beta)^{\eta}}, \tag{17-a}$$

$$h_{20} = (-\beta)^{\eta}\mathrm{Re}[K_r(0)]. \tag{17-b}$$

The two parameters β, η are chosen to approximate the magnitude, $|\hat{K}_r(s)| \approx |K_r(s)|$, and a good agreement in magnitude is achieved as shown in Fig. 9. However, significant phase error exists, but the corresponding amplitude is quite small so it is ultimately negligible when combined with $K_v(s)$. The mean-squared error of the estimate ε may be quantified as follows for typical, realistic model parameters,

$$\varepsilon = \frac{1}{Nk_0^2}\sum_{j}^{N}\left(\hat{K}_j - K_j\right)\left(\hat{K}_j^* - K_j^*\right). \tag{18}$$

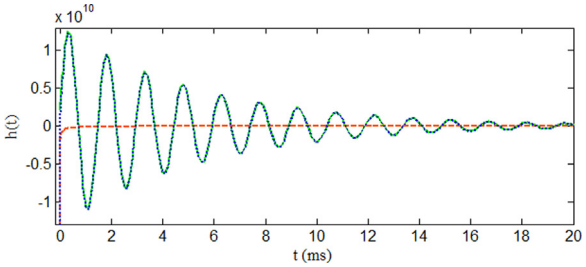

Fig. 11. Impulse response function, showing both vibratory and relaxation components. Key: ——— - Total impulse response, $h(t)$; – – – - Relaxation impulse response term, $\hat{h}_r(t)$; • • • • • - Vibratory impulse response term, $h_v(t)$.

Fig. 10 compares the $\hat{K}(s)$ estimate with the original $K(s)$ expression, obtaining $\varepsilon < 1\%$ and showing substantial improvement over a viscously damped approximation as exemplified by $K_v(s)$. Recall that the functional form of $\hat{K}_r(s)$ is chosen in Eq. (17-a) in part for its inverse Laplace transform which is given by,

$$\hat{h}_r(t) = \mathcal{L}^{-1}\left\{\frac{h_{20}}{(s-\beta)^{\eta}}\right\} = \frac{h_{20}}{\Gamma(\eta)} t^{\eta-1} e^{\beta t}, \tag{19}$$

where $\Gamma(\cdot)$ is Euler's Gamma function. This leads to the estimate form of Eq. (8), $\hat{h}(t) = h_v(t) + \hat{h}_r(t)$, which is illustrated in Fig. 11. The plot illustrates expected behavior of $h_v(t)$ as equivalent to a viscously damped second-order system response, but the effects of $\hat{h}_r(t)$ are less apparent from the impulse response. Mathematically, $\hat{h}_r(t) \to -\infty$ as $t \to 0^+$, but the physical meaning and consequences will become clear when the response to a realistic transient excitation is studied in the next section.

7. Response to a transient excitation

The following function represents a realistic displacement profile of a dynamic elastomer test machine [19] simulating a "step-like" excitation,

$$x(t) = X\left(1 - e^{-t/T}\right), \tag{20}$$

which is equivalent to a first-order system response where T is the time constant. Calculating the "step-like" response to this input requires an evaluation of the following convolution integral,

$$F(t) = \int_0^t \hat{h}(\tau) x(t-\tau) d\tau, \tag{21}$$

from which the vibratory and relaxation transient responses may be separated as,

$$F_v(t) = 2X\sqrt{A^2+B^2} \int_0^t e^{a\tau} \sin(b\tau+\theta)\left(1 - e^{-(t-\tau)/T}\right) d\tau, \tag{22-a}$$

$$\hat{F}_r(t) = \frac{h_{20} X}{\Gamma(\eta)} \int_0^t \tau^{\eta-1} e^{\beta\tau}\left(1 - e^{-(t-\tau)/T}\right) d\tau. \tag{22-b}$$

Eq. (22-a) may be expanded using trigonometric identities,

$$F_v(t) = 2X\sqrt{A^2+B^2}\left[\begin{array}{l} \cos(\theta)\left(\int_0^t e^{a\tau} \sin(b\tau) d\tau - e^{-t/T} \int_0^t e^{(a+1/T)\tau} \sin(b\tau) d\tau\right) \\ + \sin(\theta)\left(\int_0^t e^{a\tau} \cos(b\tau) d\tau - e^{-t/T} \int_0^t e^{(a+1/T)\tau} \cos(b\tau) d\tau\right) \end{array}\right], \tag{23}$$

and then integrated,

$$F_v(t) = 2X\sqrt{A^2+B^2}\left(\frac{e^{at}\sin(bt+\psi) - \sin(\psi)}{\sqrt{a^2+b^2}} - \frac{e^{at}\sin(bt+\psi_T) - e^{-t/T}\sin(\psi_T)}{\sqrt{(a+\frac{1}{T})^2+b^2}}\right), \tag{24-a}$$

$$\psi = \theta - \tan^{-1}\left(\frac{b}{a}\right), \quad \psi_T = \theta - \tan^{-1}\left(\frac{b}{a+1/T}\right). \tag{24-b,c}$$

Next, the relaxation response is divided in a similar manner,

$$\hat{F}_r(t) = \frac{h_{20} X}{\Gamma(\eta)}\left[\int_0^t \tau^{\eta-1} e^{\beta\tau} d\tau - e^{-t/T} \int_0^t \tau^{\eta-1} e^{(\beta+1/T)\tau} d\tau\right], \tag{25}$$

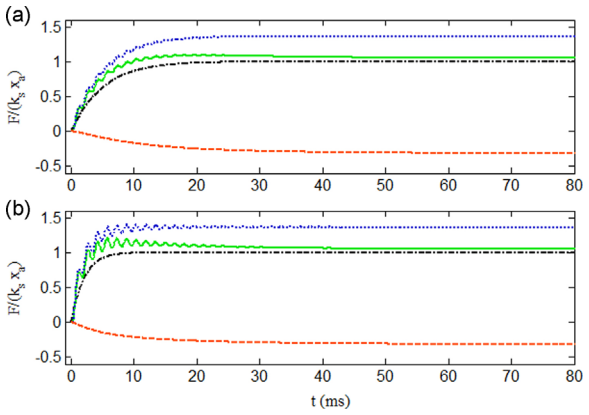

Fig. 12. Transient response of the isolator of Fig. 3(b) to "step-like" inputs with time constants of (a) $T=5$ ms and (b) $T=2$ ms. Key: ••••• - Vibratory response, $F_v(t)$; ▬ ▬ ▬ - Relaxation response, $\hat{F}_r(t)$; ▬▬ - Total response, $\hat{F}(t)$; • ▬ - Zeroth-order response, $k_0x(t)$.

and solved in terms of the incomplete Gamma function,

$$\hat{F}_r(t)=\frac{-h_{20}X}{\Gamma(\eta)}\left([(-\beta)^{-\eta}\Gamma(\eta,-\beta\tau)]_0^t-\mathrm{e}^{-t/T}\left[\left(-\beta-\frac{1}{T}\right)^{-\eta}\Gamma\left(\eta,-\left(\beta+\frac{1}{T}\right)\tau\right)\right]_0^{\tau}\right). \tag{26}$$

The solution may be further simplified in terms of the lower incomplete Gamma function [20],

$$\hat{F}_r(t)=\frac{h_{20}X}{\Gamma(\eta)}\left((-\beta)^{-\eta}\gamma(\eta,-\beta t)-\mathrm{e}^{-t/T}\left(-\beta-\frac{1}{T}\right)^{-\eta}\gamma\left(\eta,-\left(\beta+\frac{1}{T}\right)t\right)\right). \tag{27}$$

The lower incomplete gamma function may be expressed as a power series [20],

$$\gamma(a,b)=\Gamma(a)b^a\mathrm{e}^{-b}\sum_{j=0}^{\infty}\frac{b^j}{\Gamma(a+j+1)}, \tag{28-a}$$

leading to the simplification,

$$\hat{F}_r(t)=h_{20}Xt^{\eta}\mathrm{e}^{\beta t}\sum_{j=0}^{\infty}\frac{(-t)^j\left((\beta)^j-(\beta+1/T)^j\right)}{\Gamma(\eta+j+1)}. \tag{28-b}$$

Observe two-parameter Mittag-Leffler functions ($E_{\alpha,\beta}(z)$, as reported in [9,21]) in Eq. (27-a), and thus it is written more compactly as,

$$\hat{F}_r(t)=h_{20}Xt^{\eta}\mathrm{e}^{\beta t}\left[E_{1,\eta+1}(-\beta t)-E_{1,\eta+1}\left(-\left(\beta+\frac{1}{T}\right)t\right)\right]. \tag{29}$$

8. Results and discussion of the transient response

The overall transient response is compared with each term as well as the response of a model with zeroth-order system dynamics ($K(s)=k_0$) in Fig. 12, and the significance of the relaxation response (for which it is named) emerges. Two time scales are apparent. One time scale is on the order of the natural period of the internal mass (1.8 ms for this system) and governs the oscillations in the vibratory response. Conversely, the second time scale represents a slower process (about 40 ms to saturation) whereby the force transmitted from the transient event relaxes to the static equilibrium. The vibratory response behaves as a second-order system (with a pair of complex roots), while the relaxation response in some ways resembles a first-order system (with one real valued, negative root). This suggests that the fractionally damped isolator model (with a mass element) qualitatively behaves like a third-order dynamic system, even though the differential Eq. (1-a) is only of the second order.

The attributes of a fractionally damped system have significant physical ramifications for the design of vibration isolation or energy absorption components. While the spectral stiffness properties remain relevant to the design process, many applications would involve harsh transient excitation which may not reflect the frequency-domain behavior. For instance, the effect of the step time constant T on this particular system is significant. As one would expect, a quicker rise time excites the system more abruptly, producing increased oscillation and a more pronounced relaxation. These two behaviors are also strongly affected by the α_1,α_2 parameters, as seen in Fig. 13. An increased in the fractional damping order would decrease the settling time in terms of both ring-down and relaxing to the static equilibrium, but it increases the overshoot of the non-oscillatory response.

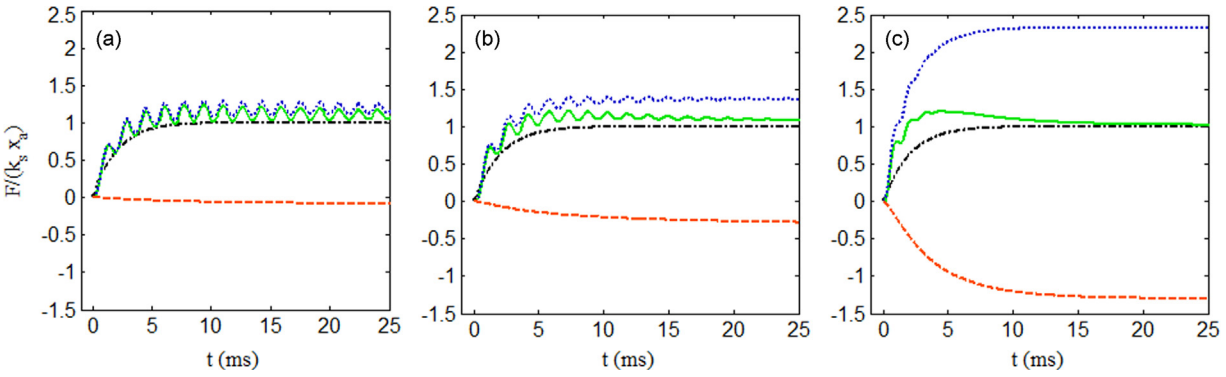

Fig. 13. Sensitivity of "step-like" responses to fractional order parameters: (a) $\alpha_1 = \alpha_2 = 0.075$, (b) $\alpha_1 = \alpha_2 = 0.15$, and (c) $\alpha_1 = \alpha_2 = 0.30$. Key: ••••• - Vibratory response, $F_v(t)$; ▬ ▬ ▬ - Relaxation response, $\hat{F}_r(t)$; ▬▬ - Total response, $\hat{F}(t)$;• ▬ - Zeroth-order response, $k_0x(t)$.

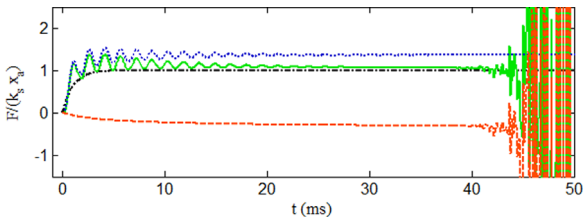

Fig. 14. Transient response showing numerical divergence using $T=1$ ms. $\alpha_1 = \alpha_2 = 2\alpha$. Key: ••••• - Vibratory response, $F_v(t)$; ▬ ▬ ▬ - Relaxation response, $\hat{F}_r(t)$; ▬▬ - Total response, $\hat{F}(t)$; • ▬ - Zeroth-order response, $k_0x(t)$.

It must be noted that the transient responses discussed in this article rely on the accurate evaluation of the Mittag-Leffler functions in Eq. (29). Due to computational limitations, these functions converge only within a finite time range, after which the error becomes excessively large. Fig. 14 illustrates this problem. The time range for which the solution converges is sensitive to both the model and its excitation parameters, most notably α_1, α_2 and T, respectively. Using a recursive definition of the Mittag-Leffler function in the context of the power series partially mitigates this problem. Since the initial transient behavior resulting from realistic excitations are within the convergent time range, an examination of more advanced methods for evaluating Mittag-Leffler functions [21] is beyond the scope of this article.

9. Conclusion

The major contribution of this article is the successful development of a minimal order system model of tuned, fractionally damped vibration isolator where the limitations of a finite element model with structural damping at the low-frequency end are overcome. This benchmark model should provide a convenient vehicle for further studies in this area. The second major contribution is the new time-frequency domain estimation procedure to calculate time-domain responses of a class of tuned, fractionally damped elastomeric joint models to realistic transient excitations. While direct analytical solutions are possible for some fractionally damped systems, the multi-domain approach proposed in this article may yield good solution estimates especially in those cases where direct solutions are infeasible. Difficulties related to the evaluation of complex, improper integrals which arise using the Residue Theorem for inverse Laplace transformation [9–11,13,14] are avoided by approximating troublesome terms with similar functions having a more well-behaved analytical behavior. This approximation achieves excellent accuracy, introducing only a minimal mean-squared error. The proposed method highlights interesting physical characteristics of a fractionally damped system, including parallel vibratory and relaxation behavior qualitatively similar to a third-order system despite starting with a second-order differential equation. Finally, this article makes a contribution to the fractional calculus based applications [9–15].

The methods proposed in this article have certain limitations resulting from the problem formulation in terms of a single degree of freedom (implying uniaxial motion) and assumptions which permit a tractable solution. Linearity is implicit to the Laplace transform, and thus the proposed analytical framework is valid for small perturbations about operating point in terms of amplitude, preload, temperature, material orientation, aging, etc. [16]. The proposed solutions provide meaningful

physical insight in the context of engineering analyses of automotive suspensions and other physical systems which employ viscoelastic isolators.

Acknowledgments

We acknowledge the member organizations of the Smart Vehicles Concepts Center (www.SmartVehicleCenter.org) such as Transportation Research Center Inc., Honda R&D Americas, Inc., F.tech R&D North America, Inc., Tenneco, Inc., Ford Motor Company, and the National Science Foundation Industry/University Cooperative Research Centers program (www.nsf.gov/eng/iip/iucrc) for supporting this work.

Appendix A. List of Symbols

a	real part of quadrant II singular point
A	real part of quadrant II residue
b	imaginary part of quadrant II singular point
B	imaginary part of quadrant II residue
c	fractional damper coefficient
C	Bromwich contour
D	derivative operator
E	two-parameter Mittag-Leffler function
h	impulse response
j	index
k	spring stiffness coefficient
K	dynamic stiffness
ℓ	integration variable
$\mathcal{L}$	Laplace transform operator
m	effective internal mass
n	common denominator of fractional orders
N	maximum number of terms
p	scaled Laplace variable
q	fractional order numerator
r	relaxation response
R	outer Bromwich contour radius
Res	simple residue
s	Laplace transform variable
t	time
T	time constant for step-like excitation
v	vibratory response
x	displacement of boundary
X	step height
y	displacement of internal mass
Z	dynamic stiffness denominator
α	fractional damper order
β	estimation root
η	estimation exponent
ε	mean squared Laplace-domain error
$\gamma(\cdot)$	lower incomplete gamma function
$\Gamma(\cdot)$	Gamma function
$\Gamma(\cdot\,,\cdot)$	upper incomplete Gamma function
θ	phase offset of vibratory response
ψ	step-like response phase offset
ξ	positive real offset
λ	singular point
ρ	inner Bromwich radius
τ	integration time

Subscripts

0	static
1, 2	coordinate of inner/outer sleeve

Superscripts

$*$	complex conjugate
$\hat{}$	estimate

References

[1] S. Kim, R. Singh, Vibration transmission through an isolator modeled by continuous system theory, *Journal of Sound and Vibration* 248 (2001) 925–953, http://dx.doi.org/10.1006/jsvi.2001.3852.

[2] S. Kim, R. Singh, Multi-dimensional characterization of vibration isolators over a wide range of frequencies, *Journal of Sound and Vibration* 245 (2001) 877–913, http://dx.doi.org/10.1006/jsvi.2001.3617.

[3] C.M. Richards, R. Singh, Characterization of rubber isolator non-linearities in the context of single and multi-degree-of-freedom experimental systems, *Journal of Sound and Vibration* 247 (2001) 807–834, http://dx.doi.org/10.1006/jsvi.2001.3759.

[4] A.F. Vakakis, S.A. Paipetis, Transient response of unidirectional vibration isolators with many degrees of freedom, *Journal of Sound and Vibration* 99 (1985) 557–562, http://dx.doi.org/10.1016/0022-460X(85)90540-1.

[5] N.C. Shekhar, H. Hatwal, A.K. Mallik, Performance of non-linear isolators and absorbers to shock excitations, *Journal of Sound and Vibration* 227 (1999) 293–307, http://dx.doi.org/10.1006/jsvi.1999.2346.

[6] S. Noll, B. Joodi, J.T. Dreyer, R. Singh, Volumetric and dynamic performance considerations of elastomeric components, *SAE International Journal of Materials and Manufacturing* 8 (2015) 953–959, http://dx.doi.org/10.4271/2015-01-2227.

[7] S. Noll, J.T. Dreyer, R. Singh, Complex eigensolutions of coupled flexural and longitudinal modes in a beam with inclined elastic supports with non-proportional damping, *Journal of Sound and Vibration* 333 (2014) 818–834, http://dx.doi.org/10.1016/j.jsv.2013.09.013.

[8] H. Jrad, J.L. Dion, F. Renaud, I. Tawfiq, M. Haddar, Experimental characterization, modeling and parametric identification of the non linear dynamic behavior of viscoelastic components, *European Journal of Mechanics A/Solids* 42 (2013) 176–187, http://dx.doi.org/10.1016/j.euromechsol.2013.05.004.

[9] R. Herrmann, *Fractional Calculus: An Introduction for Physicists*, World Scientific Publishing Co., Singapore, 2014.

[10] Y. Rossikhin, M. Shitikova, Applications of fractional calculus to dynamic problems of linear and nonlinear hereditary mechanics of solids, *Applied Mechanics Reviews* 50 (1997) 15–67, http://dx.doi.org/10.1115/1.3101682.

[11] R.L. Bagley, P.J. Torvik, A theoretical basis for the application of fractional calculus to viscoelasticity, *Journal of Rheology* 27 (1983) 201–210, http://dx.doi.org/10.1122/1.549724.

[12] N. Gil-Negrete, J. Vinolas, L. Kari, A nonlinear rubber material model combining fractional order viscoelasticity and amplitude dependent effects, *Journal of Applied Mechanics* 76 (2009) 011009, http://dx.doi.org/10.1115/1.2999454.

[13] M. Soula, T. Vinh, Y. Chevalier, Transient responses of polymers and elastomers deduced from harmonic responses, *Journal of Sound and Vibration* 205 (1997) 185–203.

[14] Y. Rossikhin, M. Shitikova, A new method for solving dynamic problems of fractional derivative viscoelasticity, *International Journal of Engineering Science* 39 (2001) 149–176, http://dx.doi.org/10.1016/S0020-7225(00)00025-2.

[15] M. Sjoberg, L. Kari, Nonlinear isolator dynamics at finite deformations: an effective hyperelastic, fractional derivative, generalized friction model, *Nonlinear Dynamics* 33 (2003) 323–336, http://dx.doi.org/10.1023/A:1026037703124.

[16] A.S. Wineman, K.R. Rajagopal, *Mechanical Response of Polymers: An Introduction*, Cambridge University Press, Cambridge, 2000.

[17] J.C. Snowdon, Mechanical four-pole parameters and their application, *Journal of Sound and Vibration* 15 (1971) 307–323, http://dx.doi.org/10.1016/0022-460X(71)90427-5.

[18] A. Edelman, H. Murakami, Polynomial roots from companion matrix eigenvalues, *Mathematics of Computation* 64 (1995) 763–776, http://dx.doi.org/10.1090/S0025-5718-1995-1262279-2.

[19] ⟨http://www.mts.com⟩. MTS Elastomer Test System Model 831.50 (accessed 8.03.15).

[20] ⟨http://dlmf.nist.gov/⟩. NIST Digital Library of Mathematical Functions, Release 1.0.10 of 2015-08-07. Online companion to [OLBC10]. (accessed 15.02.15).

[21] R. Garrappa, Numerical evaluation of two and three parameter Mittag-Leffler functions, *SIAM Journal on Numerical Analysis* 53 (2015) 1350–1369, http://dx.doi.org/10.1137/140971191.